UC Santa Barbara

UC Santa Barbara Previously Published Works

Title

Structural Insights into the Drosophila melanogaster Retinol Dehydrogenase, a Member of the Short-Chain Dehydrogenase/Reductase Family

Permalink

https://escholarship.org/uc/item/02j6s6n0

Journal

Biochemistry, 55(47)

ISSN

0006-2960

Authors

Hofmann, Lukas
Tsybovsky, Yaroslav
Alexander, Nathan S
et al.

Publication Date

2016-11-29

DOI

10.1021/acs.biochem.6b00907

Copyright Information

This work is made available under the terms of a Creative Commons Attribution License, availalbe at https://creativecommons.org/licenses/by/4.0/

Peer reviewed

eScholarship.org Powered by the California Digital Library
University of California

Author Manuscript

Author Manuscript

Author Manuscript

Author Manuscript

HHS Public Access

Author manuscript

Biochemistry. Author manuscript; available in PMC 2016 December 13.

Published in final edited form as:

Biochemistry. 2016 November 29; 55(47): 6545–6557. doi:10.1021/acs.biochem.6b00907.

Structural Insights into the *Drosophila melanogaster* Retinol Dehydrogenase, a Member of the Short-Chain Dehydrogenase/Reductase Family

Lukas Hofmann[†], **Yaroslav Tsybovsky**[†], **Nathan S. Alexander**[†], **Darwin Babino**[†], **Nicole Y. Leung**[‡], **Craig Montell**[‡], **Surajit Banerjee**[§,∥], **Johannes von Lintig**[†], and **Krzysztof Palczewski**[*,†]

[†]Department of Pharmacology and Cleveland Center for Membrane and Structural Biology, School of Medicine, Case Western Reserve University, 10900 Euclid Avenue, Cleveland, Ohio 44106, United States

[‡]Neuroscience Research Institute and Department of Molecular, Cellular, and Developmental Biology, University of California, Santa Barbara, Santa Barbara, California 93106, United States

[§]Department of Chemistry and Chemical Biology, Cornell University, Ithaca, New York 14850, United States

[∥]Northeastern Collaborative Access Team, Argonne National Laboratory, Argonne, Illinois 60439, United States

Abstract

The 11-*cis*-retinylidene chromophore of visual pigments isomerizes upon interaction with a photon, initiating a downstream cascade of signaling events that ultimately lead to visual perception. 11-*cis*-Retinylidene is regenerated through enzymatic transformations collectively called the visual cycle. The first and rate-limiting enzymatic reaction within this cycle, i.e., the reduction of all-*trans*-retinal to all-*trans*-retinol, is catalyzed by retinol dehydrogenases. Here, we determined the structure of *Drosophila melanogaster* photoreceptor retinol dehydrogenase (PDH) isoform C that belongs to the short-chain dehydrogenase/reductase (SDR) family. This is the first reported structure of a SDR that possesses this biologically important activity. Two crystal structures of the same enzyme grown under different conditions revealed a novel conformational change of the NAD^+ cofactor, likely representing a change during catalysis. Amide hydrogen–deuterium exchange of PDH demonstrated changes in the structure of the enzyme upon dinucleotide binding. In *D. melanogaster*, loss of PDH activity leads to photoreceptor degeneration that can be partially rescued by transgenic expression of human RDH12. Based on the structure of

[*]**Corresponding Author**, Department of Pharmacology, School of Medicine, Case Western Reserve University, 10900 Euclid Ave., Cleveland, OH 44106-4965. Phone: 216-368-4631. Fax: 216-368-1300. kxp65@case.edu. .

Supporting Information

The Supporting Information is available free of charge on the ACS Publications website at DOI: 10.1021/acs.biochem.6b00907.

Dimer interface statistics by residue were generated by EPPIC as were sequences of peptic fragments from PDH's primary sequence showing normalized hydrogen/deuterium uptake for apo-PDH and PDH in the presence of NAD^+ (PDF)

Illustrations involve B-factor and RMSD calculations, determination of K_d values for NAD and PDH, analysis of 3-hydroxy-retinal *in vitro* and *in vivo*, omit map representation of cofactor NAD(H), and structural alignment of PDH with DHRS4 and DHRS10 (PDF)

The authors declare no competing financial interest.

Author Manuscript Author Manuscript Author Manuscript Author Manuscript

PDH, we analyzed mutations causing Leber congenital amaurosis 13 in a homology model of human RDH12 to obtain insights into the molecular basis of RDH12 disease-causing mutations.

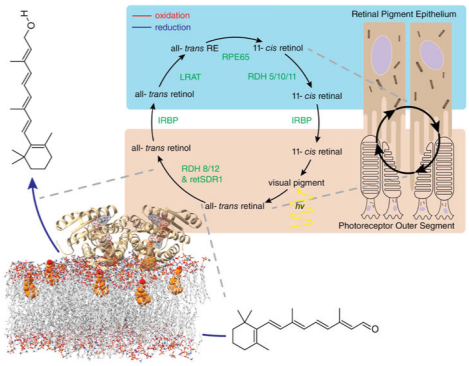

One of the key reactions involved in vitamin A metabolism and in recycling of the chromophore in vision is the NAD(P)-dependent reversible redox reaction of retinol/retinal catalyzed by alcohol dehydrogenases.[1–3] A subclass of enzymes from the SDR superfamily appears to have evolved specifically to catalyze the retinol dehydrogenase reaction.[4–8] In invertebrate photoreceptors, all-*trans*-retinylidene remains bound to opsin in a stably photoactivated form and a second photon of light is required to convert it back to 11-*cis*-3-hydroxy-retinal.[4,9–13] In flies, the chromophore is required for rhodopsin maturation, and the free chromophore can induce photoreceptor degeneration when opsin is lacking.[14] However, there is recent evidence of some enzymatic turnover of the chromophore. A mutation was discovered in a gene encoding a pigment cell-enriched NAD-dependent SDR, namely *Drosophila melanogaster* photoreceptor cell dehydrogenase (PDH), that leads to light-dependent degeneration of photoreceptor cells. Light responses and rhodopsin levels were normal in young *pdh*-deficient flies or in old mutant flies maintained in the dark.[4] However, under a light/dark cycle, *pdh*-deficient flies underwent photoreceptor degeneration with a progressive loss of retinoids and a concomitant loss of rhodopsin. Notably, this phenotype was partially rescued by ectopic expression of human RDH12 (NP_689656.2). These findings suggest that an enzymatic chromophore regeneration pathway (visual cycle) is required in flies for maintaining rhodopsin levels and the health of photoreceptors.[4,11,12]

In vertebrate vision, these redox reactions are enzymatically facilitated by retinol dehydrogenases with geometric (*cis*/*trans*) isomeric mono or dual specificities, such as RDH5, RDH8, RDH10, RDH11, and RDH12.[1] Mutations in these enzymes lead to either mild (RDH5 and RDH11) or severe (RDH12) impairments of vision or can even be lethal (RDH10) because of the requirement of retinoic acid during embryonic development.[15–21] As an example, mutations of the *RDH12* gene result in severe visual dystrophies, such as LCA13 or retinitis pigmentosa 53 (RP 53).[21] Unfortunately, no structural studies have been performed on the vertebrate enzymes, because of the inherent difficulty in expressing and purifying these proteins. Therefore, we turned to an invertebrate retinol dehydrogenase, PDH.

Author Manuscript Author Manuscript Author Manuscript Author Manuscript

Here, we present information about the crystal structure of *D. melanogaster* PDH. To the best of our knowledge, it is the first structure of a retinol dehydrogenase from the SDR family. Structural data obtained through crystallization in the presence of β-ionone suggest a novel binary conformation state of the cofactor NAD^+ prior to binding of the substrate.[22–24] Our findings also support the proposal that enzymatic activity relies on the dimerization of the protein as observed for other SDRs.[25] A model of functionally related RDH12 allowed prediction of the impact of disease-causing mutations within the catalytic domain, including the dinucleotide-binding site of the protein or the dimerization interface.

MATERIALS AND METHODS

Protein Expression and Purification

D. melanogaster pdh-c (NM_001144487.2) was cloned in a pet-45b(+) vector and expressed in BL21 *Escherichia coli*. The integrity of this expression plasmid was confirmed by sequencing. The plasmid was transformed into *E. coli* strain BL21 (DE3) (New England Biolabs, Ipswich, MA) for protein expression studies. One liter LB medium cultures containing 100 mg of ampicillin were grown at 37 °C to an OD_{600} of 0.6–0.9, after which the temperature was decreased to 25 °C and cultures were induced with 0.5 mM isopropyl β-D-1-thiogalactopyranoside. After growing for 6 h, cells were harvested by centrifugation and stored at −80 °C. Bacterial cells were lysed by four subsequent passages through a French press at 20000 psi. The lysis buffer consisted of 50 mM Tris (pH 8.0), 500 mM NaCl, and 20% glycerol. The lysate was centrifuged for 30 min at 10000*g*. The supernatant was filtered through a 0.22 μm Millex GS filter unit (Millipore, Carrigtwohill, Ireland). The filtrate was loaded onto a nickel column (cOplete His tag purification resin, Roche Diagnostic Corp., Indianapolis, IN) in the presence of 5 mM imidazole, followed by a washing step with 50 mM imidazole until no change in absorbance at 280 nm was detected. Protein then was eluted with 20 mM HEPES (pH 7.0), 500 mM NaCl, and 300 mM imidazole. The eluent was loaded onto a Sephacryl S300 HR column (GE Healthcare) equilibrated with 20 mM HEPES (pH 7.0), 680 mM NaCl, and 0.1 mM DDT. Peak fractions were combined and concentrated to 2.5 mg of protein/mL. Protein samples (≥95% pure as judged by sodium dodecyl sulfate–polyacrylamide gel electrophoresis) were placed on ice for immediate use.

Protein Crystallization, Structural Determination, and Analyses

PDHc (NP_001137959.1) was crystallized by the sitting-drop vapor-diffusion method at 4 °C in the presence of 1 mM NAD or NADH. One microliter of purified enzyme at 2.5 mg/mL in 20 mM HEPES (pH 7.0) containing 10% (w/v) glycerol and 1 mM dinucleotide was mixed with a reservoir solution containing 0.1 M BisTris (pH 6.5), 25% (w/v) PEG 3350, and either 10 mM phenol or 10 mM β-ionone in a 1:1 ratio. Cubic- or triangular-shaped crystals typically appeared within 3 days in both cases. Mature crystals were harvested, swished through a reservoir mixture containing 15% glycerol, and flash-cooled in liquid nitrogen before being exposed to X-rays.[26] Diffraction data were collected at the NE-CAT 24-ID-E beamline of the Advanced Proton Source. These data were indexed, integrated, and scaled with the XDS package.[27] The structures were determined by molecular replacement in Phaser using Protein Data Bank (PDB) entry 1B2L as the starting model.[22,28,29] Manual adjustments to each structure were made with COOT, and restrained

Author Manuscript Author Manuscript Author Manuscript Author Manuscript

refinement was performed in REFMAC5 and phenix.refine.[30–33] Structures were validated with MOLPROBITY and the wwPDB structure validation server.[34,35] A summary of the X-ray data and refinement statistics is shown in Table S1. Structural figures were prepared with PyMOL or Discovery Studio Visualizer.[36,37] Omit maps for the ligands were calculated with phenix.maps in the absence of ligands in the model file and with the initial mtz reflection file.[38]

Activity Assay of PDH Crystals

Oxidation of all-*trans*-retinol in PDH crystals was assayed by monitoring the production of all-*trans*-retinal in the presence of NAD^+.[24,39] The oxidation mixture added to the crystallization drop contained 1 mM NAD^+, 0.1 M phosphate buffer (pH 8.0), 680 mM NaCl, 10% PEG 200, 20% PEG 3350, and 244 μM all-*trans*-retinol. Reduction of all-*trans*-retinal in PDH crystals was assayed with 1 mM NADH, 0.1 M phosphate buffer (pH 5.0), 680 mM NaCl, 10% PEG 200, 20% PEG 3350, and 431 μM all-*trans*-retinal. For each redox reaction, 96 crystallization drops were incubated for 2 h at room temperature before they were harvested. The control was conducted in crystallization drops without protein. The reaction was quenched with 100 μL of methanol, and retinoids were extracted twice with 200 μL of hexane. Retinoids were separated by normal phase high-performance liquid chromatography (HPLC) in 90% hexane and 10% ethyl acetate and analyzed at both 325 and 360 nm. The reduction of 3-hydroxy-retinal followed the same procedure as described above for all-*trans*-retinal. 3-Hydroxyretinoids were obtained by enzymatically converting zeaxanthin with insect β,β-carotenoid-15,15′-oxygenase (called NINAB). Analysis and separation of 3-hydroxy-retinoids were accomplished by normal phase HPLC in 70% hexane and 30% ethyl acetate and analyzed at 325 nm. All steps were conducted under dim red light. Enzymatic activity was also tested with PDH precipitated without formation of crystals by 25% PEG 3350 and 0.1 M BTP (pH 6.5), added to the purified protein in a reaction solution of 10% PEG 200 and 20% PEG 3350 in 0.1 M BTP (pH 6.5). No activity was observed in the precipitated PDH under identical reaction conditions as observed in the redox reaction for PDH in its crystalline state.

Extensive experiments were performed to verify the catalytic activity of PDH in solution. We tested retinol dehydrogenase activity under the following conditions, all of which were analyzed with retinal, retinol, and 3-hydroxy-retinal: in the presence of CHAPS or DDM detergent micelles; in the presence of CHAPS or DDM detergent micelles with bovine albumin; in the presence of bovine albumin alone; in the presence of synthetic liposomes in which the lipid composition mimicked that of the bovine photoreceptor disc membranes, namely, 44% PE, 44% PC, and 44% PS by mass; all four isoforms [isoform A, NP_524105.2 (or NM_079381.3); isoform B, NP_730153.1 (or NM_168659.2); isoform C, NP_001137959.1 (or NM_001144487.2); isoform D, NP_001137960.1 (or NM_001144488.2)] of PDH expressed in Sf9 insect cells and purified in microsomes; all four isoforms (A–D) of PDH expressed in Sf9 insect cells and purified in microsomes in the presence of CHAPS or DDM detergent micelles; all four isoforms (A–D) of PDH expressed in Sf9 insect cells and purified in microsomes in the presence of CHAPS or DDM detergent micelles with albumin; and all four isoforms (A–D) of PDH expressed in Sf9 insect cells and

Author Manuscript Author Manuscript Author Manuscript Author Manuscript

purified in microsomes in the presence of albumin. No enzymatic activity was observed under any of these conditions.

Protein Interface Classification by Evolutionary Analysis

The dimer interface of PDH was analyzed with both PISA and EPPIC.[40–42] EPPIC classifies protein–protein interactions in a crystal lattice by including multiple-sequence alignments of homologues with ≥60% sequence identity. This classification is based on a geometric measure, namely the number of core residues and two evolutionary indicators derived from the sequence entropy of homologue sequences. Both aim to detect differential selection pressure between the interface core and either the rim or the remainder of the surface.[40] The protein–protein interaction of heterologous PDH was assessed with fast protein liquid chromatography (FPLC). PDH was analyzed either in the presence of 1 mM NAD^+ and 1 mM NADH or without dinucleotide on a Superdex 200 increase column (GE Healthcare, Pittsburgh, PA) using the equilibration buffer described in the purification protocol.

Differential Scanning Fluorimetry (DSF)

Protein stability was assessed by DSF as previously reported.[43] Briefly, the protein was diluted to a concentration of 6 μM and screened in the presence of 2 μM reporter dye, BODIPY FL L-cystine. Fifteen microliters of sample plus dye were screened against 5 μL of Hampton additive screen HT (Hampton Research, Aliso Viejo, CA). The melting temperature was determined with a Boltzmann fit. The K_d for NAD^+ was determined with DSF measurements.[43] Briefly, the melting temperature of the protein–ligand complex was determined in triplicate with a 2-fold dilution series from 18.75 to 0.009 mM NAD^+. Melting curves were fitted to the Boltzmann equation, and the resulting melting temperatures were analyzed with SigmaPlot version 11.0 according to a standard ligand binding curve.[44]

Energy Calculations

Gaussian09 software was used for quantum chemical calculations.[45] A two-layer ONIOM model[46] was employed for calculations of the protein–NAD complex, with the NAD molecule treated at the Hartree–Fock theory level with 3-21 g basis sets.[47–52] The AMBER molecular mechanics force field[53] was used for the protein. The complex was geometrically optimized, and the total ONIOM energy is reported, as well as the energy for just NAD within the complex. To obtain the energy of the two conformations of NAD in solution, the molecule was extracted from the optimized complex structures. A single-point energy calculation was then performed at the Hartree–Fock theory level with 3-21 g basis sets and water as the solvent using the polarizable continuum model.[54–70]

Amide Hydrogen–Deuterium Exchange of PDH

Amide hydrogen–deuterium exchange was performed as follows. Approximately 0.8 μg of purified PDH was diluted in 45 μL of D_2O containing 20 mM HEPES (pH 7.0) and kept on ice for 5, 10, 15, 20, or 25 min. After exposure to deuterated buffer, the exchange was terminated with ice cold quenching buffer composed of D_2O and 20 mM HEPES (pH 7.0). Ten microliters of pepsin (8.0 mg/mL, Worthington, Lakewood, NJ) was immediately added

Author Manuscript Author Manuscript Author Manuscript Author Manuscript

to the solution, and the sample was digested for 15 min on ice. Next, the sample (100 μL) was loaded onto a Luna 20 mm × 2.00 mm C18 column (Phenomenex, Torrance, CA) with a temperature-controlled Hewlett-Packard autosampler set to 4 °C. Peptides were eluted with the following gradient sequence: from 0 to 4 min, 98% H_2O with 0.1% (v/v) formic acid (A) and 2% acetonitrile with 0.1% (v/v) formic acid (B); from 4 to 12 min, 98 to 2% A. Separation was performed with an Agilent 1100 HPLC system (Agilent Technologies, Santa Clara, CA) at a flow rate of 0.2 mL/min. The eluent was injected into a Thermo Finnigan LXQ (Thermo Scientific, Waltham, MA) MS instrument equipped with an electrospray ionization source operated in a positive ion mode with other parameters adjusted as follows: activation type set to collision-induced dissociation, normalized collision energy to 35 kV, capillary temperature to 370 °C, source voltage to 5 kV, capillary voltage to 43 V, tube lens to 105 V, and MS spectra were collected over a range of *m/z* 200–2000. To avoid sample propagation from one HPLC run to another, each production run was followed by a mock injection of 10 μL of solution A with a resulting HPLC elution profile identical to the one described above. This run was followed by a 20 min equilibration run with 98% A and 2% B for 20 min. Experiments were performed at least in triplicate for each time point.

Analysis of Hydrogen–Deuterium Exchange

Peptides resulting from the pepsin digestion were identified by MS/MS by employing the online version of MassMatrix.[71] Search settings used to examine a peptic digest were as follows: precursor ion tolerance, 0.8 Da; maximal number of variable modifications allowed for each peptide sequence, 2; minimal peptide length, 4 amino acids; minimal pp score, 5; pptag score, 1.3; maximal number of combinations of different modification sites for a peptide match with modifications, 1; and maximal number of candidate peptide matches for each spectrum output in the result, 1.[72] Peptides reproducibly identified in 2 were used to construct the progress plots. Raw data in the form of relative signal intensity (percent) as a function of *m/z* were extracted with XCalibur 2.1.0. Qual Browser was used for a recently described semiautomated peak detection and deconvolution procedure performed with HDExpress software.[73,74] Briefly, after deuterium uptake was evaluated with the raw data, the value for every peptide fragment was normalized to 75% of the theoretically maximal exchangeable sites to account for the 75% deuteration accomplished experimentally (Table S2, column 4). For calculations of the maximal number of exchangeable sites, only peptide bonds were used to account for amide exchange; deuterium exchange from side chains was considered negligible and thus was not included. The maximal number of exchangeable sites was decreased by one for each P residue in a peptide sequence. Hydrogen–deuterium exchange was color-coded on the basis of the total percent of the theoretical maximal deuterium uptake at 10 min as follows: blue, 10–19%; violet, 20–29%; cyan, 30–39%; green, 40–49%; yellow, 50–59%; and orange, 60–69%.

RDH12 Modeling

The RDH12 model was calculated on the basis of the PDH crystal structure template from the SWISS-MODEL Workspace.[75–77] This model (32.48 sequence identity) yielded a GMQE value of 0.6 and a QMEAN4 of −9.66.

Author Manuscript Author Manuscript Author Manuscript Author Manuscript

RESULTS

As described in the introduction, retinol dehydrogenases are key enzymes involved the production of retinal that, in turn, is used in invertebrate and vertebrate vision, or further oxidized to retinoic acid, an important transcriptional regulator. Many years of work on vertebrate enzymes in our laboratory led to only a rudimentary determination of their expression, activity, and stereospecificity but did not produce information that could be used for structural biology approaches.[7,8,78,79] In fact, no structure of a retinol dehydrogenase from the SDR family has yet been reported. Because the *pdh-c* mutant can be rescued with the RDH12 knock-in in *D. melanogaster*, we focused on this invertebrate enzyme.[4,11,12]

The structure of PDH in the presence of NAD^+ and phenol was determined by molecular replacement using PDB entry 1B2L. PDH crystallized in the dimeric state with a Rossman fold typical of SDRs (Figure 1A–C).[22,80–83] Furthermore, the three-dimensional structure closely resembled (RMSD = 1.35 Å) that of the alcohol dehydrogenase from *Drosophila lebanonensis* (PDB entry 1B2L). The surface of the cofactor-binding site in the presence of phenol had a funnel-like shape (Figure 1). The NAD^+ entrance at the top of the funnel was characterized by hydrophilic patches, whereas the bottom entry site for the substrate was entirely hydrophobic and identically located in each monomer (Figure 1B,C). This arrangement allows a membrane-residing substrate, such as retinaldehyde, to have access to the enzyme's catalytically active site (Figure 1B,C). The C-termini of both monomers overlapped and collapsed on each other (Figure 1C). The increased *B*-factor noted for the C-terminus (Figures S1 and S2) and results of previous research regarding membrane association of the C- and N-termini of SDRs indicate that the C-terminal conformation reported here is a crystallographic artifact.[84–87]

The dissociation constant (K_d) for NAD^+ binding from DSF yielded a value of 170 ± 30 μM (Figure S3).[43] This value agrees with published K_d values for other members of the SDR family.[88,89] The ligand interaction diagram based on the structure is shown in Figure 1D.

Dimerization of short- and medium-chain dehydrogenases is a prerequisite for their activity.[25,82,90–95] Calculations of the crystallographic dimer with Proteins, Interfaces, Structures and Assemblies (PISA) indicated a biologic origin of the dimeric state (Table S3).[41] Furthermore, evolutionary analysis of the protein–protein interface with Evolutionary Protein–protein Interface Classifier (EPPIC) supported data calculated by PISA that classified the interface as being of biological origin (Figure 2 and Table S4).[40] Residues contributing to the dimer interface are depicted as sticks (Figure 2) and were evaluated with EPPIC (Table S5).[40] Gel filtration analysis of heterologous PDH in the presence or absence of dinucleotide revealed a monomeric mass under both conditions. The theoretical molecular weight (MW) determined with the ExPASy server was 29453 Da.[96] The MW of the apo state PDH as determined by gel filtration was 30.3 kDa. In the presence of NAD^+, the MW was 27.1 kDa, and in the presence of NADH, the MW was 25.6 kDa. These masses provide evidence of a monomeric form of PDH expressed in *E. coli*, as previously reported for other SDRs.[95,97] Here, the presence of a cofactor resulted in a lower molecular weight, which can be explained by a more compact structure and thus a reduced hydrodynamic radius that delayed elution from the gel filtration column. Additionally, the oligomeric state of PDH

Author Manuscript Author Manuscript Author Manuscript Author Manuscript

was analyzed by determining its MW upon gel filtration at four protein concentrations ranging from 20 to 0.5 mg/mL. The MWs of PDH indicated a sole monomeric species at all protein concentrations (Figure 2).

Purified and heterologously expressed PDH from *E. coli* or Sf9 insect cells at various concentrations was enzymatically inactive. Therefore, we assessed the activity of PDH in a crystalline state, where concentrations of the protein are significantly higher. As reported above, PDH was found in a dimeric state within crystals but not in solution. Indeed, it has been reported that SDRs remain catalytically active in a crystallized form.[24,39] Enzymatic redox reactions were performed in the crystallization drops along with the suitable cofactor. Figure 3 reveals an analysis of the reaction products by HPLC. The reduction of all-*trans*-retinal to all-*trans*-retinol is shown in Figure 3A with the corresponding spectra. Oxidation of all-*trans*-retinol to all-*trans*-retinal is depicted in Figure 3B. The naturally occurring substrate of *D. melanogaster* PDH is 3-hydroxy-retinal. Therefore, the enzymatic activity of PDH crystals was verified in the presence of this compound (Figure S4A). Accordingly, extraction and analysis of the retinoid composition from *D. melanogaster* fly heads revealed a significant reduction in the levels of both 11-*cis*- and all-*trans*-3-hydroxy-retinal in *pdh*^{1} mutants (Figure S4B).

As reported previously, the Ser-Tyr-Lys catalytic triad of SDRs is extended by a proton relay system.[82,95,98–101] Site-directed mutagenesis emphasized the importance of this catalytic triad for SDR enzymatic activity.[102] Among these three residues, Tyr is the most conserved among different family members. Panels A and B of Figure 4 show the catalytic triad Ser137-Tyr150-Lys154 of PDH in the presence of phenol (Figure 4A) and PDH crystallized in the presence of β-ionone (Figure 4B). Distances between the cofactor and the catalytic triad consistent with hydrogen bonds are depicted with dashed lines. Also, a σ–π interaction between Tyr150 and Lys154 is highlighted by an orange dashed line. The reactive hydride atom (yellow) of NADH was modeled on the basis of the NAD^+ structure used for crystallization. Cofactor isomerization as an integral characteristic of the aldehyde dehydrogenase family has been the topic of several investigations.[39,103,104] From extensive fluorescence measurements, a Mg^{2+}- and substrate-dependent cofactor isomerization reaction mechanism was proposed.[88,105] However, to date, there is no structural evidence of cofactor isomerization in the same SDR enzyme. Here, we showed an alternative binary state of NAD^+ complexed in a SDR (Figure 4B,D; PDB entry 5ILO). The conformation of the cofactor in both structures was confirmed with omit maps (Figure S5). A comparison of panels C and D of Figure 4 revealed a hydrogen bond between Ser137 and the amide group of NAD^+. This interaction was not seen in the structure when phenol was present (Figure 4C, PDB entry 5ILG). Instead, Ser137 was within hydrogen bonding distance of phenol (Figure 4A). As seen in human aldehyde dehydrogenases, isomerization resulted in the alternative configuration of the cofactor (Figure 4 and Figure S5).

Calculations indicated an energetically favored binary complex conformation of the NAD(H) cofactor as found in PDB entry 5ILO (Table S6). The binary complex conformation of NAD(H) found there is ~27.24 kJ/mol more favorable than that of the ternary complex conformation in 5ILG. The energetics of NAD(H) in vacuum and water supported previous analyses. NAD(H) in 5ILO is approximately 49.23 and 51.63 kJ/mol

Author Manuscript Author Manuscript Author Manuscript Author Manuscript

more stable than the conformation found in 5ILG in vacuum and water, respectively. Thus, an energetically favored binary state is accommodated by the cofactor prior to substrate binding. Once the substrate binds, the nicotinamide group “flips” to its accessible conformation (Figures 4 and 5). Moreover, we calculated the energies for each conformation in the presence and absence of the protein (Table S6). These data also support a nicotinamide flip (5ILO → 5ILG) upon substrate binding (Figure 5).

Hydrogen/deuterium exchange studies of PDH in the presence and absence of NAD^+ provided insights into the stabilization of the protein upon cofactor binding (Figure 6). The β-sheets within the Rossmann fold were stabilized by cofactor binding as was the loop between β-sheets 5 and 6. However, the extensive loop that connects β-sheets 6 and 7 exhibited higher flexibility. The flexibility and dynamics of the loop region between β-sheets of the Rossmann fold were in agreement with the *B*-factors calculated from the crystal structures (5ILG and 5ILO) (Figures S1 and S2). Figure S1 represents the *B*-factors of 5ILG in which the increased thermal motion of the loop between β-sheets 6 and 7 agreed with the increased flexibility shown with hydrogen/deuterium exchange and is consistent with gel filtration experiments that showed a decrease in the volume of the enzyme. The largest RMSD values between 5ILG and 5ILO were found in the loop region and the α-helical portion of PDH (Figure S2). Larger RMSD values between 5ILO and 5ILG were found in places where the *B*-factors of both structures also were elevated (Figure S2).

As indicated in the introduction, RDH12 is the human functional orthologue of PDH that reduces all-*trans*-retinal to all-*trans*-retinol in a NADP(H)-dependent manner.[7] The RDH12 model was generated with the SWISS-MODEL server based on the PDH (5ILG) crystal structure[75–77] as depicted in Figure 7. Disease-causing mutations derived from the OMIM database are listed in Table S7.

DISCUSSION

PDH provides the first structural study of a crystallized retinol dehydrogenase from the SDR family. For the first time, we obtained structural evidence of a cofactor binary state of PDH that differs from published structures of non-retinoid SDRs. Structural data combined with energy calculations indicated that the cofactor NAD(H) undergoes a conformational change upon binding of the substrate to these enzymes. Thus, isomerization of NAD(H) takes place prior to substrate binding and cofactor release. Isomerization of NAD(H) was reported previously in the context of cofactor release,[88,105–108] but such data were derived from fluorescence lifetime measurements and NMR studies of aldehyde dehydrogenase 1 (ALDH1), a member of the medium-chain dehydrogenase/reductase (MDRs) family.[109] Real-time measurements of NADH fluorescence suggested that three different species of NADH exist, namely, free NADH and two bound species of NADH with shorter and longer fluorescence lifetimes.[88,105] The species with the longer fluorescence lifetime (accessible state, 5ILG) is produced through isomerization and is dependent on substrate concentration.[88,108] On the basis of the energy calculations of 5ILG and 5ILO and the corresponding NAD(H) conformation, we conclude that the structure found in 5ILO represents the binary state of this enzyme in the absence of substrate. Thus, the amide group of the cofactor interacts via a hydrogen bridge with Ser137. Once the substrate approaches,

Author Manuscript Author Manuscript Author Manuscript Author Manuscript

the nicotinamide group undergoes a flip to its accessible conformation (5ILG) in which the hydride is within hydrogen bonding distance of the substrate (Figures 4 and 6). This mechanism is supported by enzymatic analyses of other dehydrogenases.[108,110]

DHRS4 (NP_001269916.1) and DHRS10 (NP_057330.2) are human SDRs that are dependent on NADP(H) and NAD(H), respectively. Both SDRs are known to reduce or oxidize 3-ketosteroids or 3β-hydroxy-steroids.[111–113] Figure S6 presents an alignment of the crystal structures of DHRS4 (red), DHRS10 (green), and PDH (yellow). The cofactor-binding site common to all SDR family members is nearly identical (low luminance). This finding is further supported by the low RMSD values between these structures (e.g., 1.58 Å for DHRS4 vs PDH, 1.07 Å for DHRS10 vs PDH, and 0.95 Å for DHRS4 vs DHRS10). Major differences in these structures were found only within two loop regions (high luminance) located at the substrate-binding site. The loop between β-sheets 4 and 5 showed a shortened connection in the PDH crystal structure. Moreover, the loop between β-sheets 6 and 7 revealed a completely rearranged structure as compared to the DHRS structures. This loop region also is associated with the substrate-binding site.[22] The substrate-binding loop region in PDH interacted with the opposite loop between β-sheets 5 and 6 via a hydrogen bond network and highly structured waters (S7, S17, and S20 in 5ILG). The interaction between these two opposite site loops strongly favors a substrate-binding site distant from the hydrophobic opening as depicted in Figure 1A–C.

Enzymatic assays with PDH were performed in the crystalline state in which PDH existed in a dimeric conformation. However, in solution, PDH was found exclusively in a monomeric form (Figure 2). The lack of activity in solution could thus be explained by the monomeric state of not only PDH but also other SDRs. The dependence of activity on the oligomeric state of a SDR was previously investigated by site-directed mutagenesis.[25] Results from that study agree with our data indicating that a monomeric SDR is inactive. Furthermore, this finding explains the underlying molecular mechanism of disease-causing mutations located near the dimer interface of RDH12 (Figure 7). The importance of dimerization for the activity of SDRs offers a specific target for drugs to regulate the activity of any given SDR.[25]

We made an interesting observation related to the enzymatic activity of PDH. First, the previously developed assay was validated by using bovine rod outer segment membranes that expressed high levels of retinol dehydrogenase activity.[114] This assay relies on direct detection of the retinol or retinal product, but no activity was detected in the various experimental settings described in Materials and Methods, including insect cell expression systems. This lack of activity could not be attributed to a nonproductive conformation of protein but rather to a major conformational change because the polypeptide fold is very similar to other known SDRs. When the protein was precipitated with PEG to form an amorphous material, no activity was detected either. Only when crystals were present were the enzymatic products observed. As demonstrated biochemically, PDH is monomeric even at a concentration of 20 mg/mL, but in a crystal, the dehydrogenase is present in the dimeric form where its concentration was calculated from the Matthews volume to be 826 mg/mL. For most SDRs, the dimer is obligatory for enzymatic activity,[25] but to the best of our knowledge, neither the monomeric nor the dimeric structures of the same enzyme are

Author Manuscript Author Manuscript Author Manuscript Author Manuscript

known. The most straightforward interpretation of these phenomena is that monomeric PDH is inactive and that dimerization brings together sites that then become active. Such catalytically competent dimers could have a slightly differently arranged side chain induced by dimerization. PDH crystallizes under a very narrow range of conditions, and we failed to obtain crystals in a different space group where PDH existed in a monomeric state. In insect eyes, expression of PDH could require an anchor protein that further stabilizes the dimeric form. Indeed, as demonstrated previously and here by retinoid analyses, PDH is biologically active *in vivo*.

SDRs in general have very similar folds. Now with the results of the retinol dehydrogenase structure, it is clear that there is nothing unusual about this subclass of enzymes. Thus, we can now generate models across different RDHs with greater confidence. Moreover, the interface of the PDH identified here provides additional insights. Of particular interest are those RDHs associated with human retinal diseases such as severe LCA caused by mutations in RDH12. Of the 16 listed mutations for RDH12, two cause retinitis pigmentosa 53 and 14 induce LCA 13.[115] RP 53 mutations (776delG and Ala126Val) result in a mild and late onset variant of retinitis pigmentosa.[19] These mutations are shown as balls and sticks in Figure 7. Most mutations underlying LCA were found at sites that interact with the cofactor or directly with the catalytic triad (Table S7). These results suggest that inactivation or decreased activity of the enzyme could cause this disease. Two mutations, Tyr226Cys and Thr155Ile located near the dimer interface, are known to cause LCA 13. Further progress in expressing RDH12 will be needed to validate this supposition for the last two mutations.

SUMMARY

Mutations in retinol dehydrogenases from the SDR family are associated with a broad spectrum of ocular diseases. We provide structural insights into the biochemical functioning of this class of enzymes by determining the structure of a *D. melanogaster* photoreceptor dehydrogenase, PDH. Comparisons of two structures with phenol and *β*-ionone suggest a potential substrate-induced conformational change of the cofactor NAD(H) during catalysis. Our enzymatic analyses of PDH strongly favor a native dimeric state. It was suggested that substrate binding in *D. melanogaster* alcohol dehydrogenase occurs at virtually the same cytosolic site as cofactor binding.[22] Although this could be true for soluble and hydrophilic substrates, we propose that binding of hydrophobic substrates such as retinoids occurs at the opposite site. Our finding is supported by data regarding the potential membrane-spanning N-terminus in some SDRs.[84,85,116] Hence, in a dimeric state that is crucial for the activity of PDH, the substrate entry faces the membrane, as suggested in Figure 1B. Therefore, we propose a “kiss-and-run” mechanism for the redox reactions of hydrophobic substrates that eliminates thermodynamically unfavorable extraction of retinoid from the phospholipid fraction by allowing the substrate to partially reside within the membrane. Moreover, the molecular basis of disease-causing mutations associated with severe impairments in human vision also was suggested by comparing the *D. melanogaster* dehydrogenase with its functionally related human orthologue, RDH12.

Author Manuscript Author Manuscript Author Manuscript Author Manuscript

Supplementary Material

Refer to Web version on PubMed Central for supplementary material.

ACKNOWLEDGMENTS

We thank Drs. Tivadar Orban, Marcin Golczak, and Leslie T. Webster, Jr., and members of the Palczewski laboratory for helpful comments on the manuscript. We thank Dr. Thomas Shafee for generously providing the initial concept for Figure 5.

Funding

L.H. is supported by the Swiss National Science Foundation Doc.Mobility fellowship (P1SKP3_158634). Work in the laboratory of C.M. was supported by National Institutes of Health Grant EY008117. Work in the laboratory of J.v.L. was supported by National Institutes of Health Grant EY020551. This research also was supported by National Institutes of Health Grants EY009339 (K.P.) and EY21126 (K.P.), the Arnold and Mabel Beckman Foundation, and the Canadian Institute for Advanced Research (CIFAR). K.P. is the John Hord Professor of Pharmacology. This work is based upon research conducted at the Northeastern Collaborative Access Team beamlines, which is funded by the National Institute of General Medical Sciences of the National Institutes of Health (P41 GM103403). This research used resources from the Advanced Photon Source, a U.S. Department of Energy (DOE) Office of Science User Facility operated for the DOE Office of Science by Argonne National Laboratory under Contract DEAC02-06CH11357.

ABBREVIATIONS

DHRS	dehydrogenase/reductase SDR family member
DSF	differential scanning fluorimetry
EPPIC	Evolutionary Protein–protein Interface Classifier
LCA	Leber congenital amaurosis
MW	molecular weight
PDH	photoreceptor dehydrogenase
PISA	Proteins, Interfaces, Structures and Assemblies
RDH12	retinol dehydrogenase 12
RMSD	root-mean-square deviation
SDR	short-chain dehydrogenase

REFERENCES

(1). Parker RO, Crouch RK. Retinol dehydrogenases (RDHs) in the visual cycle. Exp. Eye Res. 2010; 91:788–792. [PubMed: 20801113]

(2). Wielgus AR, Chignell CF, Ceger P, Roberts JE. Comparison of A2E cytotoxicity and phototoxicity with alltrans-retinal in human retinal pigment epithelial cells. Photochem. Photobiol. 2010; 86:781–791. [PubMed: 20497365]

(3). Saari JC, Garwin GG, Van Hooser JP, Palczewski K. Reduction of all-trans-retinal limits regeneration of visual pigment in mice. Vision Res. 1998; 38:1325–1333. [PubMed: 9667000]

(4). Wang X, Wang T, Jiao Y, von Lintig J, Montell C. Requirement for an enzymatic visual cycle in Drosophila. Curr. Biol. 2010; 20:93–102. [PubMed: 20045325]

Author Manuscript Author Manuscript Author Manuscript Author Manuscript

(5). Kiser PD, Golczak M, Palczewski K. Chemistry of the retinoid (visual) cycle. Chem. Rev. 2014; 114:194–232. [PubMed: 23905688]

(6). De Pont JJ, Daemen FJ, Bonting SL. Biochemical aspects of the visual process. VII. Equilibrium conditions in the formation of retinylidene imines. Arch. Biochem. Biophys. 1970; 140:267–274. [PubMed: 5456715]

(7). Haeseleer F, Jang GF, Imanishi Y, Driessen CA, Matsumura M, Nelson PS, Palczewski K. Dual-substrate specificity short chain retinol dehydrogenases from the vertebrate retina. J. Biol. Chem. 2002; 277:45537–45546. [PubMed: 12226107]

(8). Haeseleer F, Huang J, Lebioda L, Saari JC, Palczewski K. Molecular characterization of a novel short-chain dehydrogenase/reductase that reduces all-trans-retinal. J. Biol. Chem. 1998; 273:21790–21799. [PubMed: 9705317]

(9). Seki T, Isono K, Ozaki K, Tsukahara Y, Shibata-Katsuta Y, Ito M, Irie T, Katagiri M. The metabolic pathway of visual pigment chromophore formation in Drosophila melanogaster–all-trans (3S)-3-hydroxyretinal is formed from all-trans retinal via (3R)-3-hydroxyretinal in the dark. Eur. J. Biochem. 1998; 257:522–527. [PubMed: 9826202]

(10). Montell C. Visual transduction in Drosophila. Annu. Rev. Cell Dev. Biol. 1999; 15:231–268. [PubMed: 10611962]

(11). Montell C. Drosophila visual transduction. Trends Neurosci. 2012; 35:356–363. [PubMed: 22498302]

(12). Wang X, Wang T, Ni JD, von Lintig J, Montell C. The Drosophila visual cycle and de novo chromophore synthesis depends on rdhB. J. Neurosci. 2012; 32:3485–3491. [PubMed: 22399771]

(13). von Lintig J. Metabolism of carotenoids and retinoids related to vision. J. Biol. Chem. 2012; 287:1627–1634. [PubMed: 22074927]

(14). Voolstra O, Oberhauser V, Sumser E, Meyer NE, Maguire ME, Huber A, von Lintig J. NinaB is essential for Drosophila vision but induces retinal degeneration in opsin-deficient photoreceptors. J. Biol. Chem. 2010; 285:2130–2139. [PubMed: 19889630]

(15). Janecke AR, Thompson DA, Utermann G, Becker C, Hubner CA, Schmid E, McHenry CL, Nair AR, Ruschendorf F, Heckenlively J, Wissinger B, Nurnberg P, Gal A. Mutations in RDH12 encoding a photoreceptor cell retinol dehydrogenase cause childhood-onset severe retinal dystrophy. Nat. Genet. 2004; 36:850–854. [PubMed: 15258582]

(16). Perrault I, Hanein S, Gerber S, Barbet F, Ducroq D, Dollfus H, Hamel C, Dufier JL, Munnich A, Kaplan J, Rozet JM. Retinal dehydrogenase 12 (RDH12) mutations in leber congenital amaurosis. Am. J. Hum. Genet. 2004; 75:639–646. [PubMed: 15322982]

(17). Thompson DA, Janecke AR, Lange J, Feathers KL, Hubner CA, McHenry CL, Stockton DW, Rammesmayer G, Lupski JR, Antinolo G, Ayuso C, Baiget M, Gouras P, Heckenlively JR, den Hollander A, Jacobson SG, Lewis RA, Sieving PA, Wissinger B, Yzer S, Zrenner E, Utermann G, Gal A. Retinal degeneration associated with RDH12 mutations results from decreased 11-cis retinal synthesis due to disruption of the visual cycle. Hum. Mol. Genet. 2005; 14:3865–3875. [PubMed: 16269441]

(18). Pang JJ, Chang B, Hawes NL, Hurd RE, Davisson MT, Li J, Noorwez SM, Malhotra R, McDowell JH, Kaushal S, Hauswirth WW, Nusinowitz S, Thompson DA, Heckenlively JR. Retinal degeneration 12 (rd12): a new, spontaneously arising mouse model for human Leber congenital amaurosis (LCA). Mol. Vision. 2005; 11:152–162.

(19). Fingert JH, Oh K, Chung M, Scheetz TE, Andorf JL, Johnson RM, Sheffield VC, Stone EM. Association of a novel mutation in the retinol dehydrogenase 12 (RDH12) gene with autosomal dominant retinitis pigmentosa. Arch. Ophthalmol. 2008; 126:1301–1307. [PubMed: 18779497]

(20). Benayoun L, Spiegel R, Auslender N, Abbasi AH, Rizel L, Hujeirat Y, Salama I, Garzozi HJ, Allon-Shalev S, Ben-Yosef T. Genetic heterogeneity in two consanguineous families segregating early onset retinal degeneration: the pitfalls of homo-zygosity mapping. Am. J. Med. Genet., Part A. 2009; 149A:650–656. [PubMed: 19140180]

(21). Sun W, Gerth C, Maeda A, Lodowski DT, Van Der Kraak L, Saperstein DA, Heon E, Palczewski K. Novel RDH12 mutations associated with Leber congenital amaurosis and cone-rod dystrophy: biochemical and clinical evaluations. Vision Res. 2007; 47:2055–2066. [PubMed: 17512964]

Author Manuscript Author Manuscript Author Manuscript Author Manuscript

(22). Benach J, Atrian S, Gonzalez-Duarte R, Ladenstein R. The catalytic reaction and inhibition mechanism of Drosophila alcohol dehydrogenase: observation of an enzyme-bound NAD-ketone adduct at 1.4 A resolution by X-ray crystallography. J. Mol. Biol. 1999; 289:335–355. [PubMed: 10366509]

(23). Winberg JO, Brendskag MK, Sylte I, Lindstad RI, McKinley-McKee JS. The catalytic triad in Drosophila alcohol dehydrogenase: pH, temperature and molecular modelling studies. J. Mol. Biol. 1999; 294:601–616. [PubMed: 10610783]

(24). Tanaka N, Nonaka T, Tanabe T, Yoshimoto T, Tsuru D, Mitsui Y. Crystal structures of the binary and ternary complexes of 7 alpha-hydroxysteroid dehydrogenase from Escherichia coli. Biochemistry. 1996; 35:7715–7730. [PubMed: 8672472]

(25). Kristan K, Deluca D, Adamski J, Stojan J, Rizner TL. Dimerization and enzymatic activity of fungal 17beta-hydroxysteroid dehydrogenase from the short-chain dehydrogenase/ reductase superfamily. BMC Biochem. 2005; 6:28. [PubMed: 16359545]

(26). Pflugrath JW. Macromolecular cryocrystallography–methods for cooling and mounting protein crystals at cryogenic temperatures. Methods. 2004; 34:415–423. [PubMed: 15325658]

(27). Kabsch W. Integration, scaling, space-group assignment and post-refinement. Acta Crystallogr., Sect. D: Biol. Crystallogr. 2010; 66:133–144. [PubMed: 20124693]

(28). McCoy AJ, Grosse-Kunstleve RW, Adams PD, Winn MD, Storoni LC, Read RJ. Phaser crystallographic software. J. Appl. Crystallogr. 2007; 40:658–674. [PubMed: 19461840]

(29). Biasini M, Bienert S, Waterhouse A, Arnold K, Studer G, Schmidt T, Kiefer F, Cassarino TG, Bertoni M, Bordoli L, Schwede T. SWISS-MODEL: modelling protein tertiary and quaternary structure using evolutionary information. Nucleic Acids Res. 2014; 42:W252–258. [PubMed: 24782522]

(30). Emsley P, Lohkamp B, Scott WG, Cowtan K. Features and development of Coot. Acta Crystallogr., Sect. D: Biol. Crystallogr. 2010; 66:486–501. [PubMed: 20383002]

(31). Afonine PV, Grosse-Kunstleve RW, Echols N, Headd JJ, Moriarty NW, Mustyakimov M, Terwilliger TC, Urzhumtsev A, Zwart PH, Adams PD. Towards automated crystallographic structure refinement with phenix.refine. Acta Crystallogr., Sect. D: Biol. Crystallogr. 2012; 68:352–367. [PubMed: 22505256]

(32). Echols N, Grosse-Kunstleve RW, Afonine PV, Bunkoczi G, Chen VB, Headd JJ, McCoy AJ, Moriarty NW, Read RJ, Richardson DC, Richardson JS, Terwilliger TC, Adams PD. Graphical tools for macromolecular crystallography in PHENIX. J. Appl. Crystallogr. 2012; 45:581–586. [PubMed: 22675231]

(33). Murshudov GN, Skubak P, Lebedev AA, Pannu NS, Steiner RA, Nicholls RA, Winn MD, Long F, Vagin AA. REFMAC5 for the refinement of macromolecular crystal structures. Acta Crystallogr., Sect. D: Biol. Crystallogr. 2011; 67:355–367. [PubMed: 21460454]

(34). Chen VB, Arendall WB 3rd, Headd JJ, Keedy DA, Immormino RM, Kapral GJ, Murray LW, Richardson JS, Richardson DC. MolProbity: all-atom structure validation for macromolecular crystallography. Acta Crystallogr., Sect. D: Biol. Crystallogr. 2010; 66:12–21. [PubMed: 20057044]

(35). Read RJ, Adams PD, Arendall WB 3rd, Brunger AT, Emsley P, Joosten RP, Kleywegt GJ, Krissinel EB, Lutteke T, Otwinowski Z, Perrakis A, Richardson JS, Sheffler WH, Smith JL, Tickle IJ, Vriend G, Zwart PH. A new generation of crystallographic validation tools for the protein data bank. Structure. 2011; 19:1395–1412. [PubMed: 22000512]

(36). Discovery Studio Modeling Environment. version 4.5. Dassault Systèmes; San Diego: 2015.

(37). The PyMOL Molecular Graphics System. version 1.8. Schrodinger, LLC; Portland, OR: 2015.

(38). Adams PD, Afonine PV, Bunkoczi G, Chen VB, Davis IW, Echols N, Headd JJ, Hung LW, Kapral GJ, Grosse-Kunstleve RW, McCoy AJ, Moriarty NW, Oeffner R, Read RJ, Richardson DC, Richardson JS, Terwilliger TC, Zwart PH. PHENIX: a comprehensive Python-based system for macromolecular structure solution. Acta Crystallogr., Sect. D: Biol. Crystallogr. 2010; 66:213–221. [PubMed: 20124702]

(39). Perez-Miller SJ, Hurley TD. Coenzyme isomerization is integral to catalysis in aldehyde dehydrogenase. Biochemistry. 2003; 42:7100–7109. [PubMed: 12795606]

Author Manuscript Author Manuscript Author Manuscript Author Manuscript

(40). Duarte JM, Srebniak A, Scharer MA, Capitani G. Protein interface classification by evolutionary analysis. BMC Bioinf. 2012; 13:334.

(41). Krissinel E, Henrick K. Inference of macro-molecular assemblies from crystalline state. J. Mol. Biol. 2007; 372:774–797. [PubMed: 17681537]

(42). Krissinel E. Crystal contacts as nature's docking solutions. J. Comput. Chem. 2010; 31:133–143. [PubMed: 19421996]

(43). Hofmann L, Gulati S, Sears A, Stewart PL, Palczewski K. An effective thiol-reactive probe for differential scanning fluorimetry with a standard real-time polymerase chain reaction device. Anal. Biochem. 2016; 499:63–65. [PubMed: 26851339]

(44). SigmaPlot. version 11.0. Systat Software, Inc.; San Jose, CA:

(45). Frisch, MJ.; Trucks, GW.; Schlegel, HB.; Scuseria, GE.; Robb, MA.; Cheeseman, JR.; Scalmani, G.; Barone, V.; Mennucci, B.; Petersson, GA.; Nakatsuji, H.; Caricato, M.; Li, X.; Hratchian, HP.; Izmaylov, AF.; Bloino, J.; Zheng, G.; Sonnenberg, JL.; Hada, M.; Ehara, M.; Toyota, K.; Fukuda, R.; Hasegawa, J.; Ishida, M.; Nakajima, T.; Honda, Y.; Kitao, O.; Nakai, H.; Vreven, T.; Montgomery, JA., Jr.; Peralta, JE.; Ogliaro, F.; Bearpark, MJ.; Heyd, J.; Brothers, EN.; Kudin, KN.; Staroverov, VN.; Kobayashi, R.; Normand, J.; Raghavachari, K.; Rendell, AP.; Burant, JC.; Iyengar, SS.; Tomasi, J.; Cossi, M.; Rega, N.; Millam, NJ.; Klene, M.; Knox, JE.; Cross, JB.; Bakken, V.; Adamo, C.; Jaramillo, J.; Gomperts, R.; Stratmann, RE.; Yazyev, O.; Austin, AJ.; Cammi, R.; Pomelli, C.; Ochterski, JW.; Martin, RL.; Morokuma, K.; Zakrzewski, VG.; Voth, GA.; Salvador, P.; Dannenberg, JJ.; Dapprich, S.; Daniels, AD.; Farkas, Ö.; Foresman, JB.; Ortiz, JV.; Cioslowski, J.; Fox, DJ. Gaussian 09. Gaussian, Inc.; Wallingford, CT: 2009.

(46). Dapprich S, Komáromi I, Byun KS, Morokuma K, Frisch MJ. A new ONIOM implementation in Gaussian98. Part I. The calculation of energies, gradients, vibrational frequencies and electric field derivatives1. J. Mol. Struct.: THEOCHEM. 1999; 461–462:1–21.

(47). Binkley JS, Pople JA, Hehre WJ. Self-consistent molecular orbital methods. 21. Small split-valence basis sets for first-row elements. J. Am. Chem. Soc. 1980; 102:939–947.

(48). Gordon MS, Binkley JS, Pople JA, Pietro WJ, Hehre WJ. Self-consistent molecular-orbital methods. 22. Small split-valence basis sets for second-row elements. J. Am. Chem. Soc. 1982; 104:2797–2803.

(49). Pietro WJ, Francl MM, Hehre WJ, DeFrees DJ, Pople JA, Binkley JS. Self-consistent molecular orbital methods. 24. Supplemented small split-valence basis sets for second-row elements. J. Am. Chem. Soc. 1982; 104:5039–5048.

(50). Dobbs KD, Hehre WJ. Molecular orbital theory of the properties of inorganic and organometallic compounds 4. Extended basis sets for third-and fourth-row, main-group elements. J. Comput. Chem. 1986; 7:359–378.

(51). Dobbs KD, Hehre WJ. Molecular orbital theory of the properties of inorganic and organometallic compounds 5. Extended basis sets for first-row transition metals. J. Comput. Chem. 1987; 8:861–879.

(52). Dobbs KD, Hehre WJ. Molecular orbital theory of the properties of inorganic and organometallic compounds. 6. Extended basis sets for second-row transition metals. J. Comput. Chem. 1987; 8:880–893.

(53). Cornell WD, Cieplak P, Bayly CI, Gould IR, Merz KM, Ferguson DM, Spellmeyer DC, Fox T, Caldwell JW, Kollman PA. A Second Generation Force Field for the Simulation of Proteins, Nucleic Acids, and Organic Molecules. J. Am. Chem. Soc. 1995; 117:5179–5197.

(54). Miertuš S, Scrocco E, Tomasi J. Electrostatic interaction of a solute with a continuum. A direct utilizaion of AB initio molecular potentials for the prevision of solvent effects. Chem. Phys. 1981; 55:117–129.

(55). Miertuš S, Tomasi J. Approximate evaluations of the electrostatic free energy and internal energy changes in solution processes. Chem. Phys. 1982; 65:239–245.

(56). Pascual-ahuir JL, Silla E, Tuñon I. GEPOL: An improved description of molecular surfaces. III. A new algorithm for the computation of a solvent-excluding surface. J. Comput. Chem. 1994; 15:1127–1138.

(57). Cossi M, Barone V, Cammi R, Tomasi J. Ab initio study of solvated molecules: a new implementation of the polarizable continuum model. Chem. Phys. Lett. 1996; 255:327–335.

Author Manuscript Author Manuscript Author Manuscript Author Manuscript

(58). Barone V, Cossi M, Tomasi J. A new definition of cavities for the computation of solvation free energies by the polarizable continuum model. J. Chem. Phys. 1997; 107:3210–3221.

(59). Cossi M, Barone V, Mennucci B, Tomasi J. Ab initio study of ionic solutions by a polarizable continuum dielectric model. Chem. Phys. Lett. 1998; 286:253–260.

(60). Barone V, Cossi M, Tomasi J. Geometry optimization of molecular structures in solution by the polarizable continuum model. J. Comput. Chem. 1998; 19:404–417.

(61). Cammi R, Mennucci B, Tomasi J. Second-order Møller-Plesset analytical derivatives for the polarizable continuum model using the relaxed density approach. J. Phys. Chem. A. 1999; 103:9100–9108.

(62). Cossi M, Barone V, Robb MA. A direct procedure for the evaluation of solvent effects in MC-SCF calculations. J. Chem. Phys. 1999; 111:5295–5302.

(63). Tomasi J, Mennucci B, Cances E. The IEF version of the PCM solvation method: an overview of a new method addressed to study molecular solutes at the QM ab initio level. J. Mol. Struct.: THEOCHEM. 1999; 464:211–226.

(64). Cammi R, Mennucci B, Tomasi J. Fast evaluation of geometries and properties of excited molecules in solution: a Tamm-Dancoff model with application to 4-dimethylaminobenzonitrile. J. Phys. Chem. A. 2000; 104:5631–5637.

(65). Cossi M, Barone V. Solvent effect on vertical electronic transitions by the polarizable continuum model. J. Chem. Phys. 2000; 112:2427–2435.

(66). Cossi M, Barone V. Time-dependent density functional theory for molecules in liquid solutions. J. Chem. Phys. 2001; 115:4708–4717.

(67). Cossi M, Rega N, Scalmani G, Barone V. Polarizable dielectric model of solvation with inclusion of charge penetration effects. J. Chem. Phys. 2001; 114:5691–5701.

(68). Cossi M, Scalmani G, Rega N, Barone V. New developments in the polarizable continuum model for quantum mechanical and classical calculations on molecules in solution. J. Chem. Phys. 2002; 117:43–54.

(69). Cossi M, Rega N, Scalmani G, Barone V. Energies, structures, and electronic properties of molecules in solution with the C-PCM solvation model. J. Comput. Chem. 2003; 24:669–681. [PubMed: 12666158]

(70). Tomasi J, Mennucci B, Cammi R. Quantum mechanical continuum solvation models. Chem. Rev. 2005; 105:2999–3094. [PubMed: 16092826]

(71). Xu H, Freitas MA. MassMatrix: a database search program for rapid characterization of proteins and peptides from tandem mass spectrometry data. Proteomics. 2009; 9:1548–1555. [PubMed: 19235167]

(72). Xu H, Freitas MA. A mass accuracy sensitive probability based scoring algorithm for database searching of tandem mass spectrometry data. BMC Bioinf. 2007; 8:133.

(73). Orban T, Bereta G, Miyagi M, Wang B, Chance MR, Sousa MC, Palczewski K. Conformational changes in guanylate cyclase-activating protein 1 induced by Ca2+ and N-terminal fatty acid acylation. Structure. 2010; 18:116–126. [PubMed: 20152158]

(74). Weis DD, Engen JR, Kass IJ. Semi-automated data processing of hydrogen exchange mass spectra using HX-Express. J. Am. Soc. Mass Spectrom. 2006; 17:1700–1703. [PubMed: 16931036]

(75). Biasini M, Bienert S, Waterhouse A, Arnold K, Studer G, Schmidt T, Kiefer F, Gallo Cassarino T, Bertoni M, Bordoli L, Schwede T. SWISS-MODEL: modelling protein tertiary and quaternary structure using evolutionary information. Nucleic Acids Res. 2014; 42:W252–W258. [PubMed: 24782522]

(76). Arnold K, Bordoli L, Kopp J, Schwede T. The SWISS-MODEL workspace: a web-based environment for protein structure homology modelling. Bioinformatics. 2006; 22:195–201. [PubMed: 16301204]

(77). Benkert P, Biasini M, Schwede T. Toward the estimation of the absolute quality of individual protein structure models. Bioinformatics. 2011; 27:343–350. [PubMed: 21134891]

(78). Maeda A, Maeda T, Sun W, Zhang H, Baehr W, Palczewski K. Redundant and unique roles of retinol dehydrogenases in the mouse retina. Proc. Natl. Acad. Sci. U. S. A. 2007; 104:19565–19570. [PubMed: 18048336]

Author Manuscript Author Manuscript Author Manuscript Author Manuscript

(79). Maeda A, Golczak M, Maeda T, Palczewski K. Limited roles of Rdh8, Rdh12, and Abca4 in all-trans-retinal clearance in mouse retina. Invest. Ophthalmol. Visual Sci. 2009; 50:5435–5443. [PubMed: 19553623]

(80). Rao ST, Rossmann MG. Comparison of super-secondary structures in proteins. J. Mol. Biol. 1973; 76:241–256. [PubMed: 4737475]

(81). Persson B, Krook M, Jornvall H. Characteristics of short-chain alcohol dehydrogenases and related enzymes. Eur. J. Biochem. 1991; 200:537–543. [PubMed: 1889416]

(82). Jornvall H, Persson B, Krook M, Atrian S, Gonzalez-Duarte R, Jeffery J, Ghosh D. Short-chain dehydrogenases/reductases (SDR). Biochemistry. 1995; 34:6003–6013. [PubMed: 7742302]

(83). Benach J, Atrian S, Gonzalez-Duarte R, Ladenstein R. The refined crystal structure of Drosophila lebanonensis alcohol dehydrogenase at 1.9 A resolution. J. Mol. Biol. 1998; 282:383–399. [PubMed: 9735295]

(84). Wang J, Bongianni JK, Napoli JL. The N-terminus of retinol dehydrogenase type 1 signals cytosolic orientation in the microsomal membrane. Biochemistry. 2001; 40:12533–12540. [PubMed: 11601977]

(85). Zhang M, Hu P, Napoli JL. Elements in the N-terminal signaling sequence that determine cytosolic topology of short-chain dehydrogenases/reductases. Studies with retinol dehydrogenase type 1 and cis-retinol/androgen dehydrogenase type 1. J. Biol. Chem. 2004; 279:51482–51489. [PubMed: 15355969]

(86). Liden M, Tryggvason K, Eriksson U. Structure and function of retinol dehydrogenases of the short chain dehydrogenase/reductase family. Mol. Aspects Med. 2003; 24:403–409. [PubMed: 14585311]

(87). Lhor M, Methot M, Horchani H, Salesse C. Structure of the N-terminal segment of human retinol dehydrogenase 11 and its preferential lipid binding using model membranes. Biochim. Biophys. Acta, Biomembr. 2015; 1848:878–885.

(88). Gonnella TP, Leedahl TS, Karlstad JP, Picklo MJ. NADH fluorescence lifetime analysis of the effect of magnesium ions on ALDH2. Chem.-Biol. Interact. 2011; 191:147–152. [PubMed: 21276780]

(89). Moon HJ, Tiwari MK, Singh R, Kang YC, Lee JK. Molecular determinants of the cofactor specificity of ribitol dehydrogenase, a short-chain dehydrogenase/reductase. Appl. Environ. Microbiol. 2012; 78:3079–3086. [PubMed: 22344653]

(90). Niesen FH, Schultz L, Jadhav A, Bhatia C, Guo K, Maloney DJ, Pilka ES, Wang M, Oppermann U, Heightman TD, Simeonov A. High-affinity inhibitors of human NAD-dependent 15-hydroxyprostaglandin dehydrogenase: mechanisms of inhibition and structure-activity relationships. PLoS One. 2010; 5:e13719. [PubMed: 21072165]

(91). Ladenstein R, Tibbelin G, Karshikoff A, Atrian S, Gonzalez-Duarte R. Well ordered crystals of a short-chain alcohol dehydrogenase from Drosophila lebanonensis: re-evaluation of the crystallographic data and rotation-function analysis. Acta Crystallogr., Sect. D: Biol. Crystallogr. 1995; 51:69–72. [PubMed: 15299337]

(92). Juan E, Gonzalez-Duarte R. Purification and enzyme stability of alcohol dehydrogenase from Drosophila simulans, Drosophila virilis and Drosophila melanogaster adhS. Biochem. J. 1980; 189:105–110. [PubMed: 6779810]

(93). Winberg JO, Hovik R, McKinley-McKee JS, Juan E, Gonzalez-Duarte R. Biochemical properties of alcohol dehydrogenase from Drosophila lebanonensis. Biochem. J. 1986; 235:481–490. [PubMed: 2943270]

(94). Wuxiuer Y, Morgunova E, Cols N, Popov A, Karshikoff A, Sylte I, Gonzalez-Duarte R, Ladenstein R, Winberg JO. An intact eight-membered water chain in drosophilid alcohol dehydrogenases is essential for optimal enzyme activity. FEBS J. 2012; 279:2940–2956. [PubMed: 22741949]

(95). Mayoral JG, Leonard KT, Nouzova M, Noriega FG, Defelipe LA, Turjanski AG. Functional analysis of a mosquito short-chain dehydrogenase cluster. Arch. Insect Biochem. Physiol. 2013; 82:96–115. [PubMed: 23238893]

Author Manuscript Author Manuscript Author Manuscript Author Manuscript

(96). Wilkins MR, Gasteiger E, Bairoch A, Sanchez JC, Williams KL, Appel RD, Hochstrasser DF. Protein identification and analysis tools in the ExPASy server. Methods Mol. Biol. 1998; 112:531–552.

(97). Shafqat N, Marschall HU, Filling C, Nordling E, Wu XQ, Bjork L, Thyberg J, Martensson E, Salim S, Jornvall H, Oppermann U. Expanded substrate screenings of human and Drosophila type 10 17beta-hydroxysteroid dehydrogenases (HSDs) reveal multiple specificities in bile acid and steroid hormone metabolism: characterization of multifunctional 3alpha/7alpha/ 7beta/ 17beta/20beta/21-HSD. Biochem. J. 2003; 376:49–60. [PubMed: 12917011]

(98). Filling C, Berndt KD, Benach J, Knapp S, Prozorovski T, Nordling E, Ladenstein R, Jornvall H, Oppermann U. Critical residues for structure and catalysis in short-chain dehydrogenases/ reductases. J. Biol. Chem. 2002; 277:25677–25684. [PubMed: 11976334]

(99). Persson B, Krook M, Jornvall H. Short-chain dehydrogenases/reductases. Adv. Exp. Med. Biol. 1995; 372:383–395. [PubMed: 7484402]

(100). Oppermann UC, Persson B, Filling C, Jornvall H. Structure-function relationships of SDR hydroxysteroid dehydrogenases. Adv. Exp. Med. Biol. 1996; 414:403–415.

(101). Kallberg Y, Oppermann U, Jornvall H, Persson B. Short-chain dehydrogenase/reductase (SDR) relationships: a large family with eight clusters common to human, animal, and plant genomes. Protein Sci. 2002; 11:636–641. [PubMed: 11847285]

(102). Oppermann UC, Filling C, Berndt KD, Persson B, Benach J, Ladenstein R, Jornvall H. Active site directed mutagenesis of 3 beta/17 beta-hydroxysteroid dehydrogenase establishes differential effects on short-chain dehydrogenase/reductase reactions. Biochemistry. 1997; 36:34–40. [PubMed: 8993315]

(103). Talfournier F, Pailot A, Stines-Chaumeil C, Branlant G. Stabilization and conformational isomerization of the cofactor during the catalysis in hydrolytic ALDHs. Chem.-Biol. Interact. 2009; 178:79–83. [PubMed: 19028478]

(104). Gonzalez-Segura L, Rudino-Pinera E, Munoz-Clares RA, Horjales E. The crystal structure of a ternary complex of betaine aldehyde dehydrogenase from Pseudomonas aeruginosa Provides new insight into the reaction mechanism and shows a novel binding mode of the 2′-phosphate of NADP+ and a novel cation binding site. J. Mol. Biol. 2009; 385:542–557. [PubMed: 19013472]

(105). Gonnella TP, Keating JM, Kjemhus JA, Picklo MJ, Biggane JP. Fluorescence lifetime analysis and effect of magnesium ions on binding of NADH to human aldehyde dehydrogenase 1. Chem.-Biol. Interact. 2013; 202:85–90. [PubMed: 23295229]

(106). Blackwell LF, Motion RL, MacGibbon AK, Hardman MJ, Buckley PD. Evidence that the slow conformation change controlling NADH release from the enzyme is rate-limiting during the oxidation of propionaldehyde by aldehyde dehydrogenase. Biochem. J. 1987; 242:803–808. [PubMed: 3593277]

(107). Hammen PK, Allali-Hassani A, Hallenga K, Hurley TD, Weiner H. Multiple conformations of NAD and NADH when bound to human cytosolic and mitochondrial aldehyde dehydrogenase. Biochemistry. 2002; 41:7156–7168. [PubMed: 12033950]

(108). Bennett AF, Buckley PD, Blackwell LF. Proton release during the pre-steady-state oxidation of aldehydes by aldehyde dehydrogenase. Evidence for a rate-limiting conformational change. Biochemistry. 1982; 21:4407–4413. [PubMed: 6289881]

(109). Pares X, Farres J, Kedishvili N, Duester G. Medium- and short-chain dehydrogenase/reductase gene and protein families: Medium-chain and short-chain dehydrogenases/reductases in retinoid metabolism. Cell. Mol. Life Sci. 2008; 65:3936–3949. [PubMed: 19011747]

(110). MacGibbon AK, Blackwell LF, Buckley PD. Pre-steady-state kinetic studies on cytoplasmic sheep liver aldehyde dehydrogenase. Biochem. J. 1977; 167:469–477. [PubMed: 23112]

(111). Lukacik P, Keller B, Bunkoczi G, Kavanagh KL, Hwa Lee W, Adamski J, Oppermann U. Structural and biochemical characterization of human orphan DHRS10 reveals a novel cytosolic enzyme with steroid dehydrogenase activity. Biochem. J. 2007; 402:419–427. [PubMed: 17067289]

(112). Endo S, Maeda S, Matsunaga T, Dhagat U, El-Kabbani O, Tanaka N, Nakamura KT, Tajima K, Hara A. Molecular determinants for the stereospecific reduction of 3-ketosteroids and reactivity

Author Manuscript Author Manuscript Author Manuscript Author Manuscript

towards all-trans-retinal of a short-chain dehydrogenase/reductase (DHRS4). Arch. Biochem. Biophys. 2009; 481:183–190. [PubMed: 19056333]

(113). Matsunaga T, Endo S, Maeda S, Ishikura S, Tajima K, Tanaka N, Nakamura KT, Imamura Y, Hara A. Characterization of human DHRS4: an inducible short-chain dehydrogenase/reductase enzyme with 3beta-hydroxysteroid dehydrogenase activity. Arch. Biochem. Biophys. 2008; 477:339–347. [PubMed: 18571493]

(114). de Pont JJ, Daemen FJ, Bonting SL. Biochemical aspects of the visual process. 8. Enzymatic conversion of retinylidene imines by retinoldehydrogenase from rod outer segments. Arch. Biochem. Biophys. 1970; 140:275–285. [PubMed: 4394116]

(115). McKusick, VA. Online Mendelian Inheritance in Man, OMIM. McKusick-Nathans Institute of Genetic Medicine, Johns Hopkins University; Baltimore: 1998.

(116). Liden M, Eriksson U. Understanding retinol metabolism: structure and function of retinol dehydrogenases. J. Biol. Chem. 2006; 281:13001–13004. [PubMed: 16428379]

(117). Laskowski RA, Swindells MB. LigPlot+: multiple ligand-protein interaction diagrams for drug discovery. J. Chem. Inf. Model. 2011; 51:2778–2786. [PubMed: 21919503]

(118). Shafee, T. Wikimedia Commons. 2015. Enzyme catalysis energy levels.

Author Manuscript Author Manuscript Author Manuscript Author Manuscript

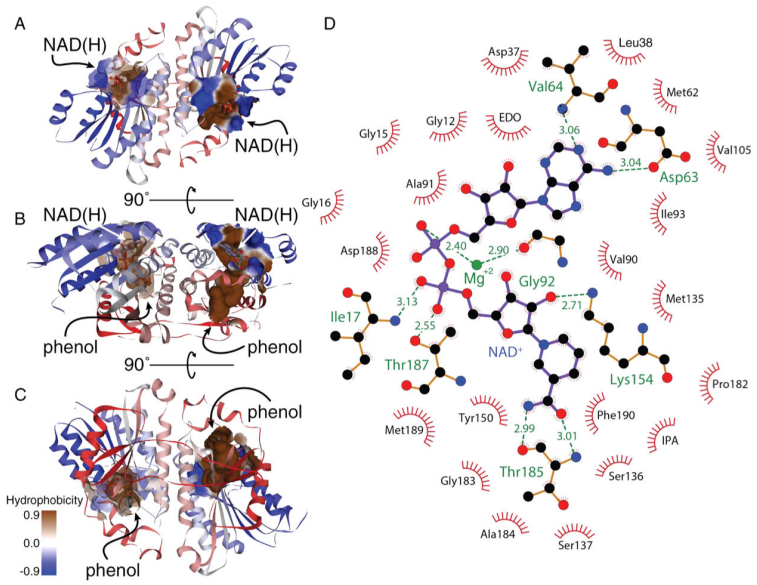

Figure 1.

Crystal structure of the PDH dimer with NAD^+ and phenol (IPA) in the active site. The left-hand panels illustrate the PDH dimer colored blue to red from the N- to C-terminus, respectively. The surface of the binding site is colored according to its hydrophobicity from blue to brown, blue for hydrophilic and brown for hydrophobic. The top view (A) shows the hydrophilic entry surface for the cofactor, and the side view (B) indicates the hydrophobic entry to the active site where phenol is located. The bottom view (C) reveals the overlapping C-termini and the entry for the substrate. Panel D displays a two-dimensional interaction diagram of the cofactor NAD^+, generated with $LigPlot^+$.[117] Phenol is abbreviated as IPA and 1,2-ethanediol as EDO. The ligands and protein side chains are represented as balls and sticks, with the ligand bonds colored purple. Hydrogen bonds (in angstroms) are displayed as green dashed lines. Protein residues making unbonded contacts with the ligand are depicted with spiked arcs.

Author Manuscript Author Manuscript Author Manuscript Author Manuscript

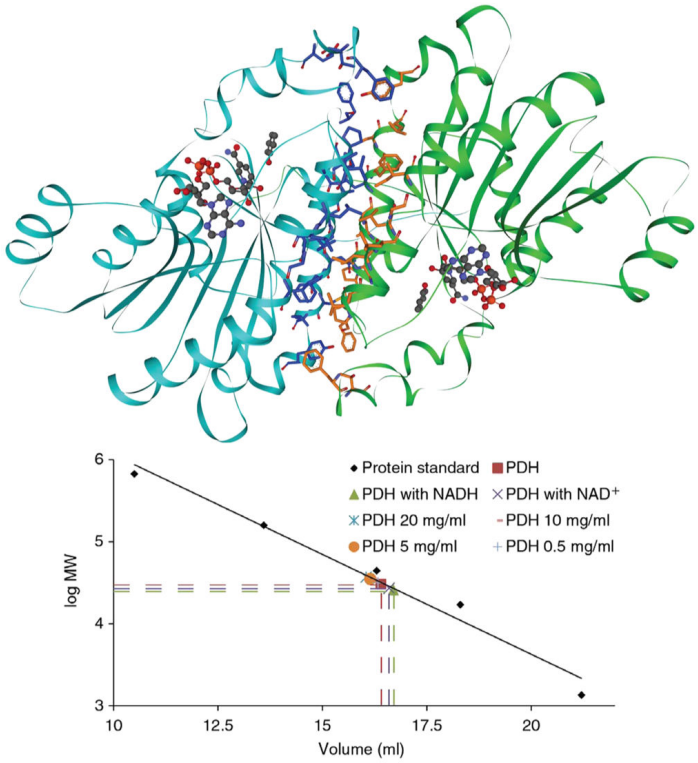

Figure 2.

Dimer interface of PDH with interacting residues and analysis of the oligomeric state upon gel filtration. The top panel illustrates the PDH dimer, in which the monomers are colored cyan for chain A and green for chain B. Cofactors and phenol are represented as balls and sticks according to their element colors. Residues contributing to the interface are colored blue for chain A or orange for chain B; these residues were verified by EPPIC (Tables S4 and S5).[40] The gel filtration analysis (bottom) was performed with the Gel Filtration Standard (model 151-1901) from Bio-Rad. Standards were thyroglobulin (bovine) (670 kDa), γ-globulin (bovine) (158 kDa), ovalbumin (chicken) (44 kDa), myoglobin (horse) (17 kDa), and vitamin B12 (1.35 kDa). PDH was injected both without (red) and with (violet) the dinucleotide NAD^+ or NADH (green). Concentration-dependent oligomerization was analyzed at PDH concentrations ranging from 20 to 0.5 mg/mL.

Author Manuscript Author Manuscript Author Manuscript Author Manuscript

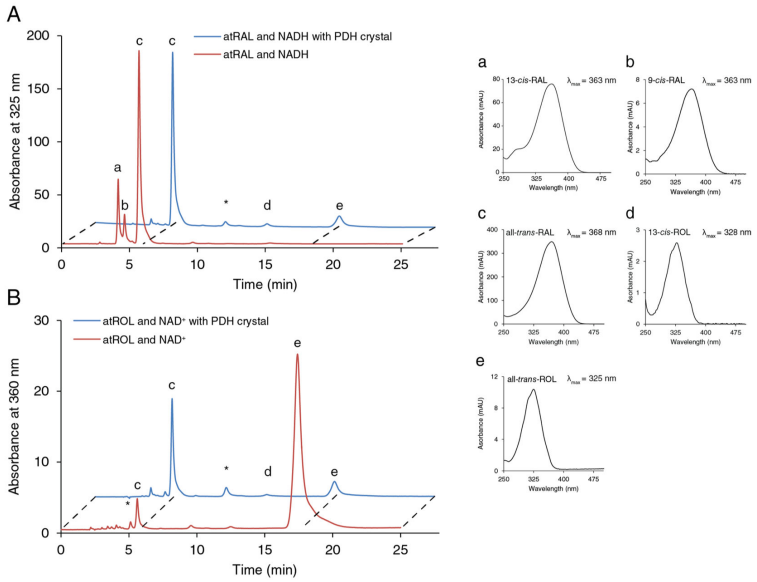

Figure 3.

HPLC analysis of PDH reaction products extracted from crystal drops. (A) Reduction of all-*trans*-retinal (c) to all-*trans*-retinol (e) in the presence (blue) and absence (red) of crystals. (B) Oxidation of all-*trans*-retinol (e) to all-*trans*-retinal (c) in the presence (blue) and absence (red) of crystals. The corresponding spectra of the different retinoid isomers a–e are shown at the right. The asterisk indicates an unidentified compound.

Author Manuscript Author Manuscript Author Manuscript Author Manuscript

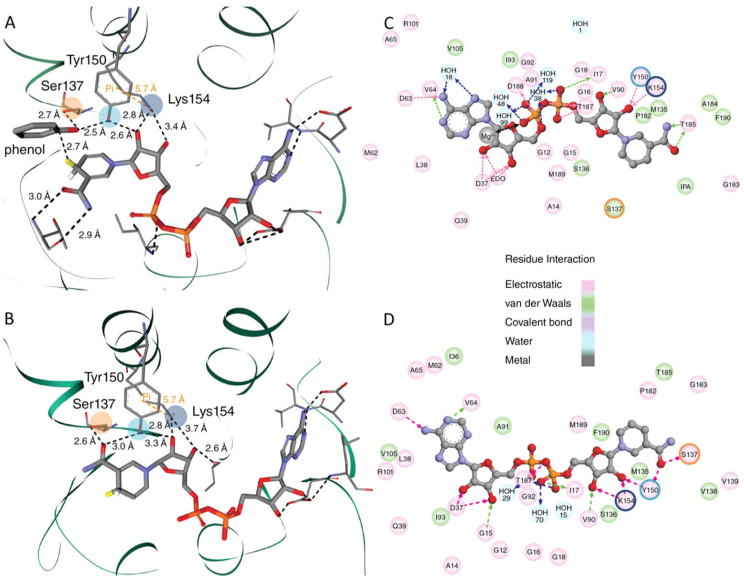

Figure 4.

Catalytic triad of PDH with phenol and cofactor in space group $P22_12_1$ (A and C) and with cofactor only in space group C121 (B and D). This two-dimensional ligand interaction diagram was generated with BIOVIA, Discovery Studio Visualizer.[36] Panels A and B show the catalytic triad with the distances in black dashed lines and the σ–π interactions colored orange. The reactive hydrogen atom of NADH was modeled on the basis of the NAD^+ structure and is colored yellow. Conformations in panels B and D reveal an NAD^+ flip in which the amide group interacts with Ser137 and Tyr150, whereas in panels A and C, the phenol interacts with Ser137, Tyr150, and the reactive hydrogen of NADH in its accessible conformation.

Author Manuscript Author Manuscript Author Manuscript Author Manuscript

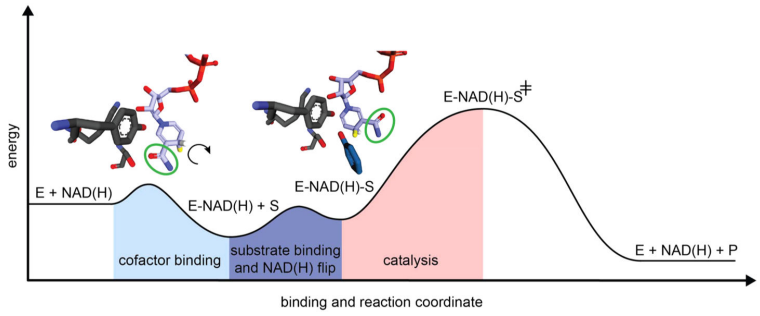

Figure 5.

Binding and reaction energy diagram of cofactor NAD(H) in the absence and presence of substrate. First, cofactor binds in its energetically favorable conformation, stabilized by a hydrogen bridge with Ser137 (light blue segment). Second, cofactor flips upon substrate binding (dark blue segment), and the hydrogen (yellow) of the cofactor is now in its accessible conformation for the phenol substrate. Third, the catalysis of hydride transfer occurs via a transition state (rose segment). Finally, the product and cofactor are released. A different version of this figure appeared in ref 118.

Author Manuscript Author Manuscript Author Manuscript Author Manuscript

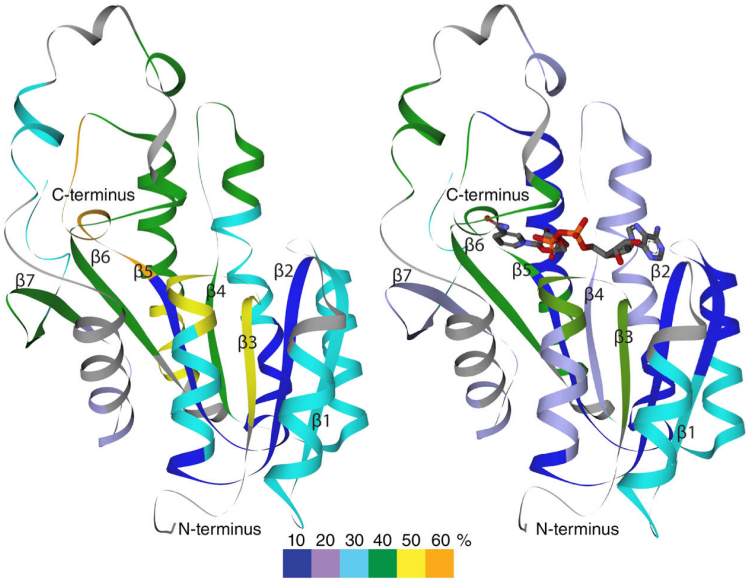

Figure 6.

PDH becomes less flexible upon dinucleotide binding as measured by hydrogen/deuterium exchange. Hydrogen/deuterium exchange rates of PDH are shown without (left) and with dinucleotide (right). PDH is colored according to the H/D exchange rates (see scale below). NAD^+ is represented as sticks in element colors. The β-sheets are numbered from 1 to 7 from the N- to C-terminus, respectively. Regions that were not evaluated are colored gray.

Author Manuscript Author Manuscript Author Manuscript Author Manuscript

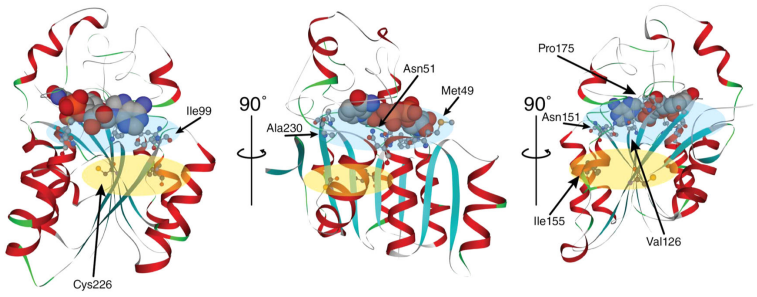

Figure 7.

LCA13 disease-causing mutations in RDH12 based on a model of the *Drosophila* PDH structure. These mutations are listed in Table S7. Mutations distant from the cofactor-binding site are highlighted with a yellow background (Tyr226Cys and Thr155Ile). Mutations interacting with the cofactor or substrate-binding site are highlighted with a blue background. RDH12 is colored according to its secondary structural elements; β-sheets are colored cyan, helices red, and loops green.